Limits on anomalous couplings of the Higgs boson to electroweak gauge bosons from LEP and the LHC

Eduard Massó[1] and Verónica Sanz[2,3]

[1]*Departament de Física and Institut de Física d'Altes Energies, Universitat Autònoma de Barcelona, E-08193 Barcelona, Spain*
[2]*Theory Division, Physics Department, CERN, CH-1211 Geneva 23, Switzerland*
[3]*Department of Physics and Astronomy, York University, Toronto, Ontario, Canada M3J 1P3*

In this paper we assume the Higgs is an elementary scalar, and study how new physics could affect its couplings to electroweak gauge bosons. Adding LHC data to LEP data provides new, more stringent limits, particularly when the Higgs to two photon decay signal strength is taken into account. We then study the effect of anomalous angular correlations in the decay to WW*. We obtain a new limit on the rare decay to photon-Z, and use it to constrain supersymmetry, to find that staus with large mixing would be most sensitive to this channel. We also use these limits to constrain radion exchange in warped extra dimensions, finding a limit on the radion mass and interaction scale of the order of TeV. Finally, we have extrapolated the current data to obtain prospects for the full 2012 data set.

I. INTRODUCTION

The new particle recently observed at around 125 GeV at LHC [1] has properties consistent with the standard model Higgs boson. More precise measurements of its couplings will provide detailed information on the mechanism of electroweak symmetry breaking (EWSB) of the standard model (SM). An impressive effort in the community is made to test the nature of the resonance [2], whether it is composite or fundamental, or even testing its scalar properties [3].

In this paper we assume that the discovered resonance is a *fundamental* scalar, and (at least partly) responsible for EWSB. Our objective is to show how LEP indirect data, and now LHC direct Higgs measurements, are shaping our understanding of new physics from the so-far only resonance uncovered at the LHC, which we call "the Higgs" below.

We now proceed to set the notation used in the paper, from the Higgs sector to the basis of effective operators adopted throughout the paper.

In the SM, the Higgs particle H forms part of a $SU(2)_L$ doublet,

$$\Phi = \frac{1}{\sqrt{2}}\begin{pmatrix} \phi_1 + i\phi_2 \\ v + H + i\phi_3 \end{pmatrix}, \qquad (1)$$

where v is the vacuum expectation value of the neutral part of the doublet. The term in the Lagrangian responsible for the gauge bosons masses is

$$(D_\mu \Phi)^\dagger (D^\mu \Phi). \qquad (2)$$

Here the covariant derivative is given by

$$D_\mu \Phi = \left(\partial_\mu + i\frac{g}{2}\tau^a W_\mu^a + i\frac{g'}{2}B_\mu \right)\Phi, \qquad (3)$$

where τ^a are the Pauli matrices, g and g' are the $SU(2)_L$ and $U(1)_Y$ gauge couplings, respectively, and the corresponding gauge fields V are W_μ^a and B_μ.

EWSB gives rise at the same time to the generation of the weak gauge boson masses and to their couplings HVV,

$$\frac{g^2 v^2}{4} W_\mu^+ W^{-\mu}\left(1 + 2\frac{H}{v} \right) + \frac{1}{2}\frac{(g^2 + g'^2)v^2}{4} Z_\mu$$
$$\times Z^\mu\left(1 + 2\frac{H}{v} \right), \qquad (4)$$

where we have defined the fields $W^\pm = (W^1 \mp iW^2)/\sqrt{2}$. In Eq. (4), valid at tree level, we appreciate the presence of the custodial symmetry: in the limit $g' \to 0$, the masses of the three weak gauge bosons are equal, and the couplings to the Higgs are identical.

Since the EWSB mechanism is at the origin of the mass of W and Z and at the same time determines the couplings of the Higgs to them, the study of the couplings of the Higgs to electroweak bosons is expected to shed light on the EWSB mechanism. With this in mind, in this paper we deal with the coupling of the Higgs to electroweak bosons. Along the same philosophy, we are not considering anomalous coupling of the Higgs with the gluon G. This is a simplification, but also motivated by the tight direct bounds on strong production from the LHC. New physics able to modify the HGG coupling would be necessarily charged under $SU(3)_c$. An example would be a new heavy color triplet, such as the stop in supersymmetry. This colored particle would have an important effect in the Higgs couplings to both gluons and photons, and their effect is very correlated such that the stop effect can be rephrased in terms of higher order operators [4].

As we said, in this paper we assume that the particle observed at LHC at 125 GeV is the fundamental Higgs particle H, but we also suppose that there is new physics at

higher energies which might induce some relatively small changes in the H properties. Specifically, we will concentrate on the HVV couplings which are not of the form shown in (4). We will also assume that the effects beyond the SM can be described in terms of effective Lagrangians valid up to a high-energy scale Λ.

How heavy has to be the new physics to fall into this analysis, based on effective operators? All processes concerning the Higgs at the LHC have relatively small energy exchange. For example, in the dominating production mechanism, gluon fusion, one can write the factorization

$$\sigma_{\text{prod}}(gg \to H) \simeq \frac{\pi^2}{8m_H}\Gamma(H \to gg)\delta(\hat{s} - m_H^2), \quad (5)$$

which is just based on the narrow width approximation [5]. Therefore, in Higgs production through gluon fusion, the typical exchange in momentum is $Q^2 \simeq m_H^2$, and new physics at a scale $\Lambda \gg m_H$ would lead to a sensible effective theory. The same reasoning follows for other production mechanisms, such as vector bosons fusion or associated production.

II. THE LANGUAGE OF EFFECTIVE OPERATORS

Let us consider the effective Lagrangian

$$\mathcal{L}_{\text{eff}} = \sum_i \frac{f_i}{\Lambda^2}\mathcal{O}_i \quad (6)$$

with the subset of operators $\mathcal{O}_i$ which modify the HVV vertices.[1] These operators have been investigated by Refs. [7–9] before the LHC discovery, and by Ref. [10] after the Higgs discovery. The operators $\mathcal{O}_i$ are dimension-six and thus they are suppressed by a high-energy scale Λ. Throughout our paper we use the convention and notations which were used in Refs. [9,10].

The list of operators is not long. We start with operators containing the scalar field Φ and its derivative. There is a first operator which breaks custodial symmetry at tree level,

$$\mathcal{O}_{\Phi,1} = (D_\mu\Phi)^\dagger\Phi \quad \Phi^\dagger(D^\mu\Phi) \quad (7)$$

and there are two which preserve it,[2]

$$\mathcal{O}_{\Phi,2} = \frac{1}{2}\partial_\mu(\Phi^\dagger\Phi)\,\partial^\mu(\Phi^\dagger\Phi), \quad (8)$$

$$\mathcal{O}_{\Phi,4} = (\Phi^\dagger\Phi)\quad(D_\mu\Phi)^\dagger(D^\mu\Phi). \quad (9)$$

The list continues with five operators involving the scalar field and the field strengths:

$$B_{\mu\nu} = \partial_\mu B_\nu - \partial_\nu B_\mu, \quad (10)$$

$$W_{\mu\nu}^a = \partial_\mu W_\nu^a - \partial_\nu W_\mu^a - g\epsilon^{abc}W_\mu^b W_\nu^c. \quad (11)$$

In this paper, we use the rescaled field strengths $\hat{B}_{\mu\nu} = i(g'/2)B_{\mu\nu}$ and $\hat{W}_{\mu\nu} = i(g/2)\tau^a W_{\mu\nu}^a$.

There is a first operator that contributes at tree level to the $B - W^3$ mixing,

$$\mathcal{O}_{BW} = \Phi^\dagger\hat{W}^{\mu\nu}\Phi\hat{B}_{\mu\nu}, \quad (12)$$

and four other operators,

$$\mathcal{O}_W = (D_\mu\Phi)^\dagger\hat{W}^{\mu\nu}(D_\nu\Phi), \quad (13)$$

$$\mathcal{O}_B = (D_\mu\Phi)^\dagger(D_\nu\Phi)\hat{B}^{\mu\nu}, \quad (14)$$

$$\mathcal{O}_{WW} = \Phi^\dagger\hat{W}^{\mu\nu}\hat{W}_{\mu\nu}\Phi = -\frac{g^2}{4}(\Phi^\dagger\Phi)W^{a\mu\nu}W_{\mu\nu}^a, \quad (15)$$

$$\mathcal{O}_{BB} = (\Phi^\dagger\Phi)\hat{B}^{\mu\nu}\hat{B}_{\mu\nu}. \quad (16)$$

Let us now discuss which operators we will consider in our paper. First, the two operators (7) and (12) have a tree level effect on precision electroweak observables and therefore are subject to very strict constraints. Because of this reason, we will not consider them: the LHC is not providing more information on those operators. Second, the operators (8) and (9) affect the HVV couplings through a Higgs field renormalization, so that the induced effect has the same form as in (4), namely it is of the form $HW^\mu W_\mu$ and $HZ^\mu Z_\mu$. Such normalization effects will be rather hard to extract in the near future,[3] so we will not consider these two operators here. In summary, in this paper we will work out the consequences of the four operators $\mathcal{O}_W$, $\mathcal{O}_B$, $\mathcal{O}_{WW}$, $\mathcal{O}_{BB}$, contributing to $\mathcal{L}_{\text{eff}}$ in (6) when added to the SM Lagrangian, with a total Lagrangian

$$\mathcal{L} = \mathcal{L}_{\text{SM}} + \mathcal{L}_{\text{eff}}. \quad (17)$$

III. CONSTRAINTS FROM PRECISION ELECTROWEAK PHYSICS

The four operators (13)–(16) contribute to precision electroweak observables measured for example at LEP and at Tevatron. The observed experimental values severely constrain the presence of those operators.

Let us start with data coming from measurements of Z-pole observables, W-mass, and low energy experiments. The standard way to proceed is to use the S, T, and U parameters to find the bounds.[4] The operators we are considering contribute at the one-loop level to S, T, and

---

[1]For bounds on other operators not involving the Higgs see Ref. [6].

[2]Note that these two operators are not independent, as they are related by a nonlinear field redefinition, $\Phi \to \Phi(1 + \alpha\Phi^\dagger\Phi)$, with a suitable parameter α; see Ref. [10].

[3]See Ref. [11] for a study of the LHC limits on these operators.

[4]We shall use the definitions of these parameters in the PDG [12].

U. The corresponding expressions have been calculated in Ref. [13]. They read

$$
\alpha S = \frac{e^2}{96\pi^2}\Big\{3[\epsilon_W + \epsilon_B]\frac{m_H^2}{v^2}\log\frac{\Lambda^2}{m_H^2} + 2[(5c^2 - 2)\epsilon_W
$$
$$
- (5c^2 - 3)\epsilon_B]\frac{m_Z^2}{v^2}\log\frac{\Lambda^2}{m_H^2} - [(22c^2 - 1)\epsilon_W
$$
$$
- (30c^2 + 1)\epsilon_B]\frac{m_Z^2}{v^2}\log\frac{\Lambda^2}{m_Z^2} - 24[c^2\epsilon_{WW}
$$
$$
+ s^2\epsilon_{BB}]\frac{m_Z^2}{v^2}\log\frac{\Lambda^2}{m_H^2}\Big\}, \tag{18}
$$

$$
\alpha T = \frac{3e^2}{64\pi^2}\frac{1}{c^2}\Big\{\epsilon_B\frac{m_H^2}{v^2}\log\frac{\Lambda^2}{m_H^2} + [c^2\epsilon_W + \epsilon_B]\frac{m_Z^2}{v^2}\log\frac{\Lambda^2}{m_H^2}
$$
$$
+ [2c^2\epsilon_W + (3c^2 - 1)\epsilon_B]\frac{m_Z^2}{v^2}\log\frac{\Lambda^2}{m_Z^2}\Big\}, \tag{19}
$$

$$
\alpha U = \frac{e^2}{48\pi^2}s^2\Big\{[4\epsilon_W - 5\epsilon_B]\frac{m_Z^2}{v^2}\log\frac{\Lambda^2}{m_H^2}
$$
$$
+ [-2\epsilon_W + 5\epsilon_B]\frac{m_Z^2}{v^2}\log\frac{\Lambda^2}{m_Z^2}\Big\}. \tag{20}
$$

Here we have defined

$$
\epsilon_i = f_i\frac{v^2}{\Lambda^2}, \tag{21}
$$

for $i = W, B, WW, BB$. The quantities e, $c = \cos\theta_W$ and $s = \sin\theta_W$ are $\overline{MS}$ couplings. To have limits on the ϵ_i using S, T, U in (18)–(20) we need to specify the value of Λ in the logarithm; we shall use $\Lambda = 1$ TeV. Changing the value of Λ does not change very much the limits we shall find on the different ϵ_i; in fact, as we increase Λ, the limits on ϵ_i tighten. The presence of the logarithm is because our operators affect S, T, U at a one-loop order. As we will see, the induced ϵ_i for observables at LHC are at tree level and do not have such logarithm of Λ.

The adimensional parameters ϵ_i encode the strength coefficient f_i of the operators as well as the ratio among the Fermi scale v and the new physics scale Λ. An alternative, which is also used in the current literature, would be to specify the scale Λ and show the limits on f_i. If one chooses $\Lambda = 1$ TeV, any limit on a specific ϵ_i shown in our paper translates into a limit on the corresponding f_i given by $f_i \simeq 16\epsilon_i$.

We stress that the loops contributing to S, T, and U, as well as to the other observables contain quadratic divergences which cancel because we are using an effective Lagrangian that contains gauge-invariant operators [7,8]. Only the logarithmic terms remain; we have kept only this logarithmic part of the calculation and not the constant terms.

Let us now move to the physics of the triple gauge-boson vertices V^3, since the operators $\mathcal{O}_W$ and $\mathcal{O}_B$ have

contributions at tree level, and therefore LEP2 measurements can constrain them. In the presence of these two operators, the relevant part of the total Lagrangian (17) contains three parameters, Δg_1^Z, $\Delta\kappa_Z$, and $\Delta\kappa_\gamma$

$$
\mathcal{L}_{V^3} = i\frac{ec}{s}[(1 + \Delta g_1^Z)(W_{\mu\nu}^- W^{+\mu} - W_{\mu\nu}^+ W_\mu^-)Z^\nu
$$
$$
+ (1 + \Delta\kappa_Z)W_\mu^- W_\nu^+ Z^{\mu\nu}] + ie[(W_{\mu\nu}^- W^{+\mu}
$$
$$
- W_{\mu\nu}^+ W_\mu^-)A^\nu + (1 + \Delta\kappa_\gamma)W_\mu^- W_\nu^+ A^{\mu\nu}], \tag{22}
$$

where we have defined the field strengths corresponding to the Abelian part,

$$
V^{\mu\nu} = \partial^\mu V^\nu - \partial^\nu V^\mu \tag{23}
$$

with $V = \gamma, W, Z$.

The deviations from the standard model due to the new parameters are given by [7]

$$
\Delta g_1^Z = \frac{e^2}{8s^2c^2}\epsilon_W, \tag{24}
$$

$$
\Delta\kappa_Z = \frac{e^2}{8s^2c^2}(c^2\epsilon_W - s^2\epsilon_B), \tag{25}
$$

$$
\Delta\kappa_\gamma = \frac{e^2}{8s^2}(\epsilon_W + \epsilon_B). \tag{26}
$$

A. Limits in the one parameter space

To bound each operator we first use the recent limits found by Erler [14] on the electroweak parameters S, T, and U. The result of the fit to electroweak data for $M_H = 125$ GeV is

$$
S = 0.00 \pm 0.10, \quad T = 0.02 \pm 0.11, \quad U = 0.04 \pm 0.09. \tag{27}
$$

Imposing these experimental limits to each operator separately, i.e., not allowing for cancellations between different operators, and working at 95% C.L., we obtain

$$
-1.9 \leq \epsilon_W \leq 2.3, \tag{28}
$$

$$
-0.90 \leq \epsilon_B \leq 0.90, \tag{29}
$$

$$
-1.5 \leq \epsilon_{WW} \leq 1.5, \tag{30}
$$

$$
-5.6 \leq \epsilon_{BB} \leq 5.6. \tag{31}
$$

Actually, it is S and T which restrict the ϵ_i parameters, with U not playing a role. Indeed, one expects the new physics effect on U to be suppressed [15] by v^2/Λ^2 with respect to T.

Now we would like to find the analogous bounds coming from V^3 data. We use the LEP2 experimental limits on Δg_1^Z, $\Delta\kappa_Z$, and $\Delta\kappa_\gamma$ as compiled by the PDG [12],
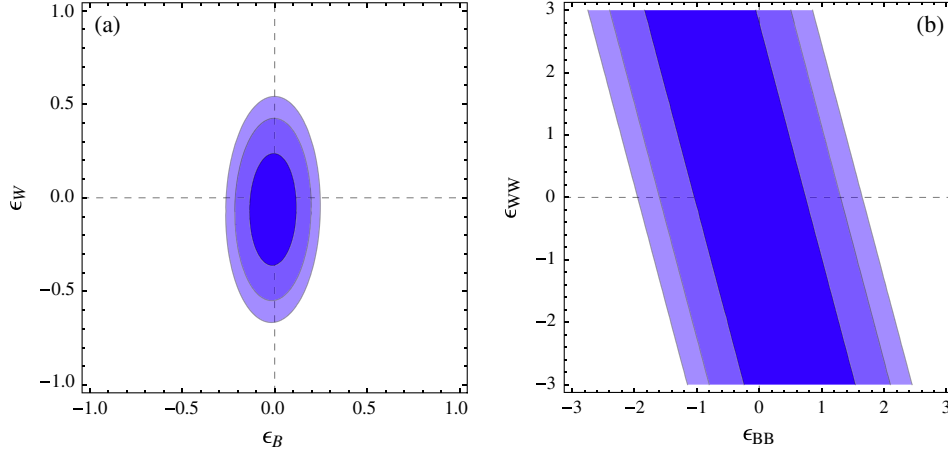
FIG. 1 (color online).   The 68%, 95%, and 99% C.L. allowed regions in the parameters (ϵ_W, ϵ_B) and $(\epsilon_{WW}, \epsilon_{BB})$. We use the limits (37) with the U parameter fixed to zero as well as (32) and (34).

$$1 + \Delta g_1^Z = 0.984^{+0.022}_{-0.019}, \tag{32}$$

$$1 + \Delta \kappa_Z = 0.924^{+0.067}_{-0.061}, \tag{33}$$

$$1 + \Delta \kappa_\gamma = 0.973^{+0.044}_{-0.045}. \tag{34}$$

We should stress that each of these bounds is obtained setting the other two parameters to their SM values, i.e., equal to zero. Strictly speaking, the way these limits are extracted do not lead rigorously to individual bounds on ϵ_W and ϵ_B. For example, if we wish to get a limit on ϵ_W with $\epsilon_B = 0$, we should allow the three parameters in (24)–(26) to be nonzero, in the proportions indicated by the equations and then compare with experiment.

However, there is a way out of this problem. Since the experimental bound on Δg_1^Z leads to the tightest constraint, and this depends only on ϵ_W, it is a very good approximation to neglect ϵ_W in (25) and (26). Actually, when we make this approximation, we realize that (34) is more constraining than (33), so we can use only the limit coming from (34). With these approximations, we can get bounds on the strength of the effective operators. Working at 95% C.L., we obtain

$$-0.73 \leq \epsilon_W \leq 0.38, \tag{35}$$

$$-2.1 \leq \epsilon_B \leq 1.04. \tag{36}$$

We finally stress that LHC is also providing experimental data [16] on the V^3 vertices which in the future may be competitive with the old LEP2 data we use here.

B. Limits on the two parameter space

Although we do not expect fine-tuned cancellations among the contributions of different operators, it is interesting to see what happens when we consider two operators at the same time. Since the structure of the operators $\mathcal{O}_W$ and $\mathcal{O}_B$ is very similar, we shall consider the situation where they are both generated by new physics existing at higher energy scales and investigate the bounds coming from precision electroweak physics, including LEP2. For the same reasons we shall also consider the case where we have the simultaneous effects of $\mathcal{O}_{WW}$ and $\mathcal{O}_{BB}$. In Secs. VI and VII, we will provide examples of this common generation in the case of supersymmetry and extra dimensions.

For this exercise we shall use the LEP2 data, Eqs. (32) and (34), as well as the limits on S and T when $U = 0$ is fixed [17],

$$S = 0.02 \pm 0.08, \qquad T = 0.05 \pm 0.07, \tag{37}$$

with a correlation coefficient of 0.89. These values are obtained using the same data input as in Ref. [14].

Figure 1 shows the 68%, 95%, and 99% confidence level (C.L.) allowed regions in the (ϵ_W, ϵ_B) and $(\epsilon_{WW}, \epsilon_{BB})$ planes. As expected, the contours in (ϵ_W, ϵ_B) are ellipses. However, the contours in the plane $(\epsilon_{WW}, \epsilon_{BB})$ are stripes because the corresponding operators on the one hand do not modify the V^3 vertices, and on the other hand they are custodial preserving, and thus there is a single constraint coming from the S parameter.

IV. LHC BOUNDS

In this section we shall study the constraints on the operators (13)–(16) that can be obtained by analyzing Higgs *decays* at LHC. We do not consider the effect on the production, although the associated production channels ($q\bar{q} \rightarrow V^* \rightarrow V + H$) and the vector boson fusion ($qq' \rightarrow qq'VV \rightarrow qq'H$) are sensitive to the operators considered in this paper. The reason is that the production is largely dominated by gluon fusion processes; hence, the decay rates are the best way to bound the operators.

A. The translation between effective operators and Higgs couplings

The contributions of our operators to the HWW and HZZ vertices have a different form than the SM expression (4). One can write

$$\Delta \mathcal{L}_{HZZ} = g^{(1)}_{HZZ} Z_{\mu\nu} Z^\mu \partial^\nu H + g^{(2)}_{HZZ} Z_{\mu\nu} Z^{\mu\nu} H,$$
$$\Delta \mathcal{L}_{HWW} = g^{(1)}_{HWW} (W^+_{\mu\nu} W^{-\mu} \partial^\nu H + \text{H.c.})$$
$$+ g^{(2)}_{HWW} W^+_{\mu\nu} W^{-\mu\nu} H, \tag{38}$$

where we have defined the field strengths corresponding to the Abelian part,

$$V^{\mu\nu} = \partial^\mu V^\nu - \partial^\nu V^\mu. \tag{39}$$

The couplings in (38) are easily obtained [7,9,10],

$$g^{(1)}_{HZZ} = \frac{e^2}{4v}\left(\frac{1}{c^2}\epsilon_B + \frac{1}{s^2}\epsilon_W\right),$$
$$g^{(2)}_{HZZ} = -\frac{e^2}{4v}\left(\frac{s^2}{c^2}\epsilon_{BB} + \frac{c^2}{s^2}\epsilon_{WW}\right), \tag{40}$$
$$g^{(1)}_{HWW} = \frac{e^2}{4v}\frac{1}{s^2}\epsilon_W, \qquad g^{(2)}_{HWW} = -\frac{e^2}{2v}\frac{1}{s^2}\epsilon_{WW}.$$

In addition, one obtains couplings of the Higgs H to two photons and to one photon and one Z-boson

$$\Delta \mathcal{L}_{HAA} = g_{HAA} A_{\mu\nu} A^{\mu\nu} H,$$
$$\Delta \mathcal{L}_{HAZ} = g^{(1)}_{HAZ} A_{\mu\nu} Z^\mu \partial^\nu H + g^{(2)}_{HAZ} A_{\mu\nu} Z^{\mu\nu} H, \tag{41}$$

where

$$g_{HAA} = -\frac{e^2}{4v}(\epsilon_{BB} + \epsilon_{WW}),$$
$$g^{(1)}_{HAZ} = \frac{e^2}{4v}\frac{1}{sc}(-\epsilon_B + \epsilon_W), \tag{42}$$
$$g^{(2)}_{HAZ} = \frac{e^2}{2v}\left(\frac{s}{c}\epsilon_{BB} - \frac{c}{s}\epsilon_{WW}\right).$$

B. The impact of Higgs data in the effective operator basis

The LHC measures the signal significance in each channel in terms of the *signal strength* $\hat{\mu}$:

$$\hat{\mu}_i = \frac{[\sum_j \epsilon_{ij}\sigma_{j\to H} \times \text{Br}(H \to i)]_{\text{observed}}}{[\sum_j \epsilon_{ij}\sigma_{j\to H} \times \text{Br}(H \to i)]_{\text{SM}}}, \tag{43}$$

where $i = 1, \ldots, N_{ch}$ with N_{ch} the number of channels, the label j in the cross section, $\sigma_{j\to H}$, is due to the fact that some final states are summed over different Higgs production processes, labeled with j. ϵ_{ij} denotes the efficiency under experimental cuts.

For this study we will use the signal strengths shown in Fig. 2, which correspond to CMS and ATLAS combinations
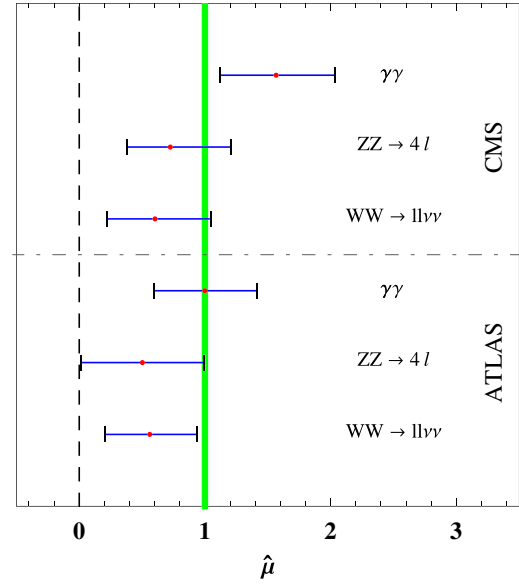

FIG. 2 (color online). Signal strengths used in this paper. The upper three correspond to CMS data, and the last three numbers are the ATLAS combination results.

of 7 and 8 TeV runs, in the channels of $\gamma\gamma$, and fully leptonic WW^* and ZZ^*. For limits from LEP, see Ref. [18].

1. The diphoton channel

The operators ϵ_{WW} and ϵ_{BB} affect the decay of $H \to \gamma\gamma$, with no relative factor. The cuts applied on the photon channel [19,20] will not induce a difference in efficiencies when the operators are switched on because the structure of the vertex is the same, and only the overall normalization is changed.

To do the simulation of the effective operators, we created a new model in FEYNRULES [21], adding to the SM the new operators in Eqs. (40) and (42). We then interfaced with MADGRAPH [22] using the UFO model format [23]. We incorporated hadronization and showering effects using PYTHIA [24] and detector effects with DELPHES [25]. In our simulation, jets are always anti-k_T jets of size $R = 0.5$.

One can extract bounds on ϵ_{WW} and ϵ_{BB} at the 95% C.L. using Fig. 3, where the effect of the operators is shown relative to the SM. The bounds are shown in Table I, to compare with those coming from precision measurements in Sec. III, Eqs. (28)–(31), (35), and (36). The direct measurement of the Higgs to two photon surpasses the sensitivity from LEP limits on ϵ_{WW} and ϵ_{BB} by a factor $\mathcal{O}(10)$.

Before moving onto the other channels, let us comment about a simplification made in extracting the bounds. We are using the combined data from 7 and 8 TeV center-of-mass energies. The production cross sections are obviously slightly different, but the effect on the ratios of total cross sections, the signal strength, is negligible. Hence, our simplified analysis with combined data is valid.
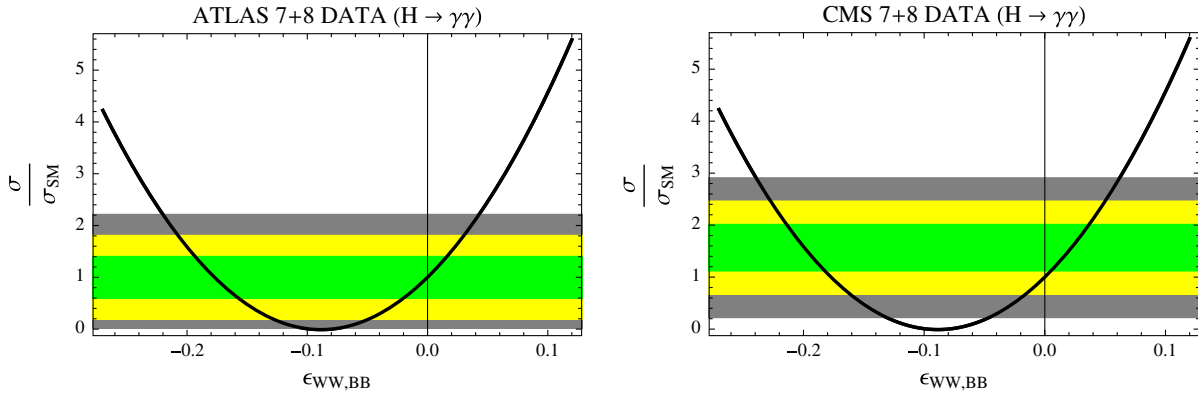
FIG. 3 (color online). The total cross section as a function of the operators $\epsilon_{WW,BB}$ for ATLAS (left) and CMS (right) combined data. Green, yellow, and gray areas correspond to 1, 2, and 3 σ, respectively.

2. The WW and ZZ channels

In the WW channel, the information of the angular correlation between the two leptons is used to reject background. Since our new operators in Eq. (40) have different Lorentz structure, one could imagine a substantial difference in the angular distribution, which is indeed a way to determine the spin of the Higgs resonance.

Nevertheless we argue that, irrespective of the Lorentz structure of the vertex, the difference between the SM and the new vertex is small because it involves the spin-zero Higgs. To explain this effect, let us take the much simpler case of on-shell WW production. The Higgs is a scalar, which determines the combinations of helicity in the outgoing W's as $\epsilon_{W^-}^+ \epsilon_{W^+}^- + \epsilon_{W^-}^- \epsilon_{W^+}^+ - \epsilon_{W^-}^0 \epsilon_{W^+}^0$ [26]. One can then relate those polarizations to the dilepton angular distributions as shown in Ref. [26], to find that the distribution in terms of the azimuthal angle difference ($\Delta\Phi_{\ell\ell}$) is a decreasing function. As we move into the real situation, where at least one of the W's is off shell, this behavior qualitatively persists. This can be seen in an explicit simulation of the effect of the different vertices, as shown in Fig. 4. We plotted the angular distribution of the dilepton system when vertices of the SM, $g^{(1)}$ and $g^{(2)}$ types are switched on. The distributions are very similar because the fact that the leptons tend to be produced in parallel is a consequence of the spin of the Higgs. Note, though, that one could try to extract the Lorentz structure of the vertex in a linear collider [27,28], and in the vector boson fusion channel [29], or possibly with more data [30,31].

TABLE I. One-parameter bounds from the $H \to \gamma\gamma$, WW^*, and ZZ^* channels at the LHC.

Quantity	Bound	Source
ϵ_{WW}, ϵ_{BB}	$[-0.21, 0.03]$	Diphoton-ATLAS
ϵ_{WW}, ϵ_{BB}	$[-0.23, 0.05]$	Diphoton-CMS
ϵ_W	$[-1.3, 18.5]$	WW-CMS and ATLAS
ϵ_B	> -9.7	ZZ-CMS

Although the differences are small, we would like to quantify them by implementing the ATLAS [32] and CMS [33] searches for the Higgs to two leptons. Our implementation of the ATLAS analysis starts with a selection of events with two opposite-sign, opposite-flavor leptons with $p_T^{\ell_1,\ell_2} > 25$, 15 GeV in the central region, and invariant mass 50 GeV $> m_{\ell\ell} > 10$ GeV. Quality and isolation criteria are applied at the level of DELPHES simulation. We will focus on the zero- and one- and two-jet analysis. The jets are asked to have $p_T > 25$, 30 GeV in the central, forward region. In the zero-jet region, the final cuts applied are

$$E_{T,\text{rel}}^{\text{miss}} > 25 \text{ GeV}, \qquad p_T^{\ell\ell} > 30 \text{ GeV}, \quad \text{and} \quad |\Delta\Phi_{\ell\ell}| < 1.8,$$
(44)

whereas in the one-jet case, there is an extra cut,

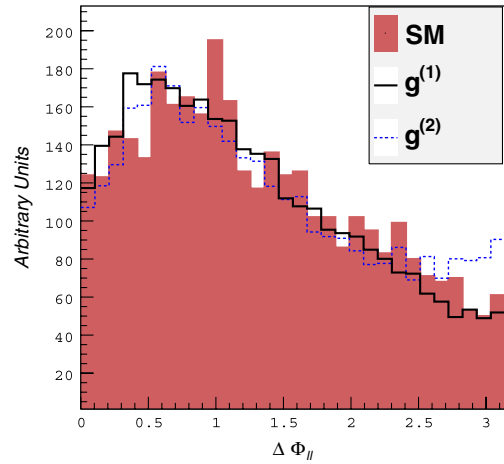$$\vec{p}_T^{\,\ell\ell} + \vec{p}_T^{\,j} + \vec{E}_T^{\text{miss}} < 30 \text{ GeV}$$
(45)

FIG. 4 (color online). The effect of the different Lorentz structures in the dilepton angular distributions. We plot the $\Delta\Phi_{\ell\ell}$ distribution for the three vertices considered here.
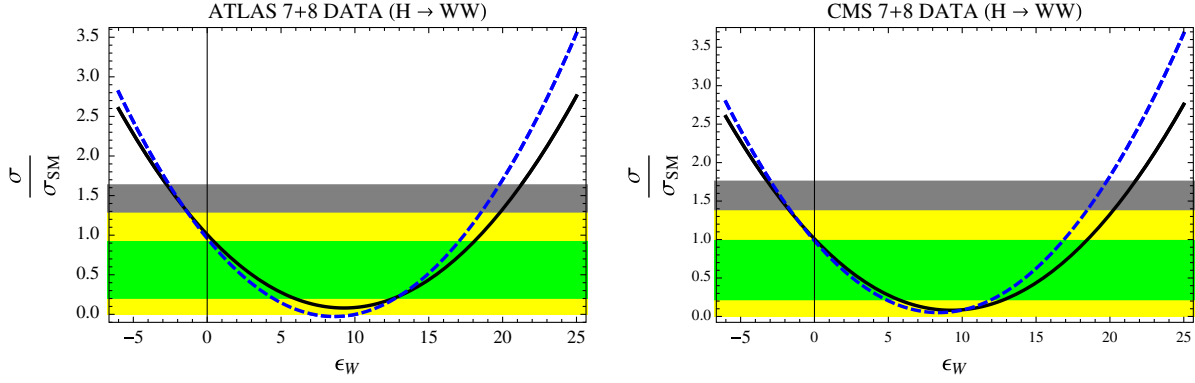
FIG. 5 (color online). The total cross section as a function of the operator ϵ_W for ATLAS (left) and CMS (right) combined data. Green, yellow, and gray areas correspond to 1, 2, and 3 σ, respectively. The blue-dashed line corresponds to having the efficiencies effect into account.

besides a b-tag veto. Finally, a cut on m_T between 93.75 and 125 GeV is applied.

We also simulate the corresponding CMS search. CMS cuts are very similar to ATLAS, but now $p_T^{\ell\ell} > 45$ GeV, $m_{\ell\ell} \in [12, 45]$ GeV, $\Delta\Phi_{\ell\ell} < 1.6$, and $m_T \in [80, 125]$ GeV. Let us note that the $\Delta\Phi_{\ell\ell}$ cut is correlated to the other two cuts.

We present our results in Fig. 5 for the case of the operators $\epsilon_{W,B}$, which generate couplings of the type $g^{(1)}$. We do not use the WW channel to constrain the $\epsilon_{WW,BB}$ operators, as the $\gamma\gamma$ limits are much better. The black line is the value of $\hat{\mu}$ without cuts. The dashed-blue line corresponds to the same quantity with cuts taken into account. The slight difference among lines reflects the little distinction between the SM and the $g^{(1)}$ type of couplings in the cuts applied.

Finally, we looked into the Higgs to four leptons, via ZZ^*. ATLAS [34] and CMS [35] use quite different techniques for the time being. ATLAS is a cut based analysis, which essentially asks for $m_{2\ell}$ and $m_{4\ell}$ in the range of the Z and H masses. CMS uses a rather sophisticated multivariate analysis called MELA, which is based in four angular observables and one invariant mass. As we discussed for the WW^* case, we do not expect any sizable effect on efficiencies due to the new couplings, less so in the case of ATLAS ZZ^* analysis. In the global fit presented later on, we will use information from all these channels, but the $\gamma\gamma$ will be the observable from the LHC leading the constraints, with the WW and ZZ channels, limited by statistics, playing a less important role.

V. COMBINED CONSTRAINTS ON ANOMALOUS COUPLINGS

Now we would like to repeat the exercise we did at the end of Sec. III, namely, to find the constraints in the planes $(\epsilon_{WW}, \epsilon_{BB})$ and (ϵ_W, ϵ_B). Of course, it is expected that adding the recent LHC data will improve these constraints,

but the degree of amelioration is something we would like to evaluate in this section.

In Fig. 6(a) we see the results on (ϵ_W, ϵ_B). Comparing with Fig. 1(a) we notice there is no substantial improvement with the LHC so far, to the extent that the ellipse from LEP and from the combined LEP + LHC are basically the same. In Sec. VIII we will explain why we do not expect much improvement from the full 2012 LHC data set for those parameters.

In Fig. 6(b) we see the results on $(\epsilon_{WW}, \epsilon_{BB})$; in this case the improvement is dramatic since we go from constraints in the form of stripes in Fig. 1(b) to contour ellipses in Fig. 6(b). Since the constraints on $(\epsilon_{WW}$ and $\epsilon_{BB})$ are dominated by the $\gamma\gamma$ channel, the constraints are better presented in terms of the orthogonal combinations $\epsilon_{WW} + \epsilon_{BB}$ and $\epsilon_{WW} - \epsilon_{BB}$. Also, due to the fact that the present $\gamma\gamma$ data exceed the theoretical SM prediction by more than one sigma, there are actually two constrained regions in Fig. 6(b).

In Fig. 6 we also show the constraints coming from LEP alone and the ones coming from the different LHC channels. We hope this clarifies even more the role of the separate experimental constraints. In Fig. 6(b) we show how the stripe coming from LEP [basically the one of Fig. 1(b)] nicely complements the stripe coming from the $\gamma\gamma$ LHC channel. The narrower, darker, horizontal stripe is the CMS data; the wider, lighter, stripe is the ATLAS data. We do not show the stripes corresponding to WW and ZZ LHC channels because they are much more loose, and actually the stripe borders are outside the region of parameters we display in Fig. 6(b). In Fig. 6(a) we show the role of the WW LHC channel (darker region) and the ZZ LHC channel (lighter region).

VI. LIMITS ON THE COUPLING OF THE HIGGS TO PHOTON-Z

Higher order operators can induce a coupling of the Higgs to a Z and a photon, as shown in Eq. (42). The decay rate is then given by
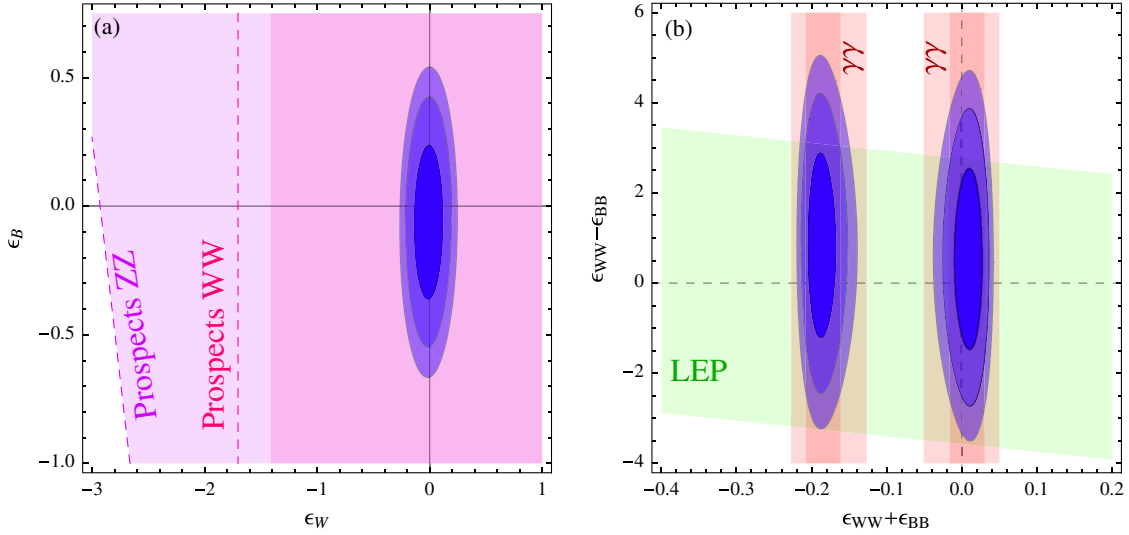
FIG. 6 (color online).   Constraints from electroweak precision data and LHC data on the coefficients (ϵ_W, ϵ_B) and $(\epsilon_{WW} + \epsilon_{BB}, \epsilon_{WW} - \epsilon_{BB})$. In blue, the 99%, 95%, and 68% C.L. combined constraints. We show the individual constraints coming from LEP and from LHC (regions corresponding to $\Delta\chi^2 = 3.84$) and the prospects (see text).
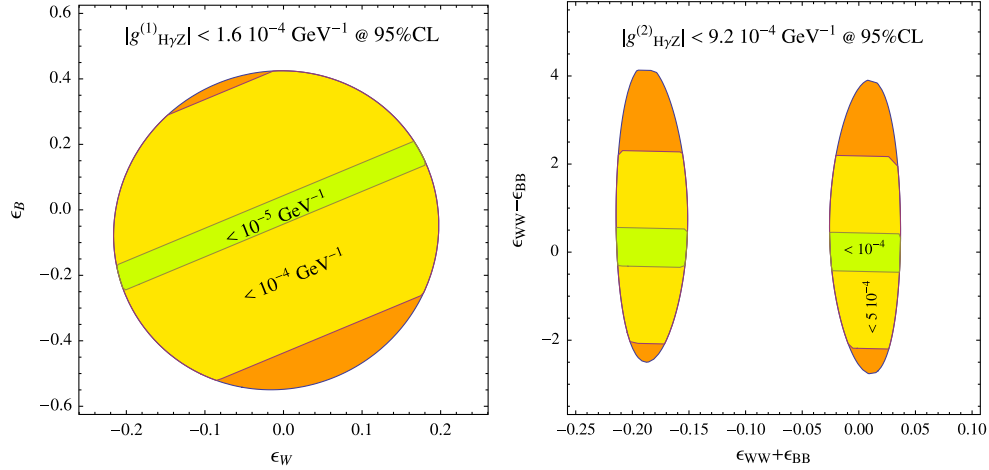

FIG. 7 (color online).   Limits on the coupling of the Higgs to γZ in the (ϵ_W, ϵ_B) (left) and $(\epsilon_{WW}, \epsilon_{BB})$ (right) parameter space. The current limit on the generated couplings $g^{(1,2)}$ is shown in the plot, as well as slices of tighter upper limits.

$$\Gamma(H \to \gamma Z) = \frac{m_H^3}{16\pi}\left(1 - \frac{m_Z^2}{m_H^2}\right)^3 |g_{HAZ}^{(1)} + 2g_{HAZ}^{(2)} + \kappa_{\text{SM}}|^2. \tag{46}$$

The SM contribution is $\kappa_{\text{SM}} \simeq -4.1 \times 10^{-5}$ GeV^{-1}, where we have included the W and top loops. For a discussion on the expected LHC sensitivity to direct measurements, see Ref. [36].

In Fig. 7 we show lines of fixed bounds for $g_{HAZ}^{(1)}$ and $g_{HAZ}^{(2)}$ in the $(\epsilon_{WW}, \epsilon_{BB})$ and (ϵ_W, ϵ_B) parameter space, respectively. One can infer then limits in the 95% C.L. which read

$$|g_{HAZ}^{(1)}| < 1.6 \times 10^{-4} \text{ GeV}^{-1}, \tag{47}$$

$$|g_{HAZ}^{(2)}| < 9.2 \times 10^{-4} \text{ GeV}^{-1}, \tag{48}$$

or, equivalently,

$$\Gamma(H \to \gamma Z) < 1.0 \times 10^{-4}(1.3 \times 10^{-2}) \text{ GeV}, \tag{49}$$

depending on which operator is switched on, $g^{(1)}$ ($g^{(2)}$).[5] Note that the SM contribution is very small, $\Gamma(H \to Z\gamma)_{\text{SM}} \simeq 6 \times 10^{-6}$ GeV. In Fig. 7 we also show contours of $g_{HAZ}^{(1)} < 10^{-4}$, 10^{-5} GeV^{-1} and $g_{HAZ}^{(2)} < 5 \times 10^{-4}$, 10^{-4} GeV^{-1}.

---

[5]Note that our limits on $g^{(2)}$ are more conservative than those in Ref. [29].
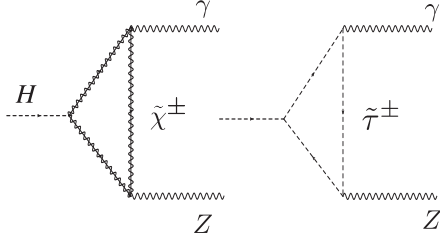
FIG. 8. Chargino/stau contribution to loop diagrams leading to the anomalous coupling $A_{\mu\nu}Z^{\mu\nu}H$.

One could interpret the bounds on the decay in terms of new physics generated by, for example, supersymmetry. A coupling of the kind $g^{(2)}HA_{\mu\nu}Z^{\mu\nu}$ could be generated by a loop of charged Higgses, charginos, and staus as shown in the diagram of Fig. 8 [37]. We consider the interpretation in terms of exclusively electroweak states, neglecting the effect of stops, which should be heavy enough as to not influence this vertex, and neither the gluon coupling to Higgses. We will also work in the decoupling limit of the two-Higgs doublet model, as the observed Higgs and the bounds on the pseudoscalar Higgs are consistent with this assumption. In this case, the charged Higgs contribution is 2 orders of magnitude smaller than the W contribution $[g^{(2)}_{H^{\pm}} = \alpha/(24\sqrt{2}\pi sc\upsilon) \simeq 7 \times 10^{-7} \text{ Gev}^{-1}]$, hence this analysis provides no information on the charged Higgs.

In the limit of a heavy chargino, its contribution would be given by

$$g^{(2)}_{HAZ}(\tilde{\chi}^{\pm}) = -\frac{\alpha}{3\sqrt{2}s\upsilon}\frac{m_Z}{m_{\tilde{\chi}^{\pm}}}g_{Z\tilde{\chi}^{\pm}\tilde{\chi}^{\mp}}g_{H\tilde{\chi}^{\pm}\tilde{\chi}^{\mp}}, \quad (50)$$

where $g_{(Z,H)\tilde{\chi}^{\pm}\tilde{\chi}^{\mp}}$ are the couplings of the Z and H to the charginos, and they are bounded by $\lesssim 1$. This implies that the chargino contribution is about 1 order of magnitude smaller than the SM one for $m_{\tilde{\chi}^{\pm}} \gtrsim \upsilon$.

The situation for staus is more promising, provided the staus have a large left-right mixing. In this limit the induced coupling can be estimated as

$$g^{(2)}_{HAZ}(\tilde{\tau}) \simeq -\frac{\alpha}{6\sqrt{2}sc\upsilon}\left(\frac{m_{\text{LR}}}{m_{\tilde{\tau}_\ell}}\right)^2, \quad (51)$$

where $\tilde{\tau}_\ell$ is the lightest stau, and m_{LR} is the off-diagonal mass term, $m_\tau(A_{\tilde{\tau}} + \mu/\tan_\beta)$, and we have taken the limit in the loop integrals of heavy stau. The limit on the anomalous coupling can then be translated in

$$m_{\text{LR}} \lesssim 30 m_{\tilde{\tau}_\ell}. \quad (52)$$

By going through this exercise, we see that the current data set it not sensitive to charginos and charged Higgs via the indirect probes we are discussing here [38]. In the case of the stau, the sensitivity depends largely on the amount of mixing between the two staus. But note that a large $m_{\text{LR}}/m_{\tilde{\tau}_\ell}$ means that there would be a large gap between the two stau physical states, possibly getting into the dangerous region of charge breaking minima if $m^2_{\tilde{\tau}_\ell} < 0$.

VII. CONSTRAINING NEW PHYSICS: A TOY EXAMPLE

As a final illustration of the effect of the bounds on effective operators on UV models, we use the example of a radion in warped extra dimensions. We follow closely the discussion in Ref. [39].

The coupling of the radion R to massless gauge fields is loop induced and given by

$$\mathcal{L} \supset \frac{R}{L\Lambda}\left(\frac{1}{g^2}\hat{W}^{\mu\nu}\hat{W}_{\mu\nu} + \frac{1}{g'^2}\hat{B}^{\mu\nu}\hat{B}_{\mu\nu}\right), \quad (53)$$

where we are neglecting the localized kinetic terms and trace anomalies. Here $L = \log(M_P/\text{TeV}) \simeq 30$ in the usual Randall-Sundrum (RS) model, but can be smaller in the little Randall-Sundrum (LRS) [40]. For example, with a cutoff of order 100 TeV, one would expect $L \simeq 5$. Note that after EWSB, this coupling receives an extra contribution, suppressed by the order of the effective volume of the extra dimension, i.e., $\mathcal{O}(30)$.

Assuming there is no Higgs-curvature mixing, and that the Higgs is localized on the IR brane, the coupling of the radion to the Higgs would be given by

$$\mathcal{L} \supset \frac{2R}{\Lambda}m^2_H\Phi^\dagger\Phi. \quad (54)$$

Integrating out the heavy radion leads to the effective operator

$$\epsilon_{BB} \simeq -\left(2\frac{m_H\upsilon}{\Lambda m_R}\right)^2 \frac{1}{Lg'^2} = \frac{g^2}{g'^2}\epsilon_{WW}. \quad (55)$$

The typical energies at which we are probing those anomalous couplings are $Q^2 \simeq m^2_H$; hence, in our expansion of the radion dynamics, we are neglecting terms of order m^2_H/m^2_R. In Fig. 9, we present the limit in terms of
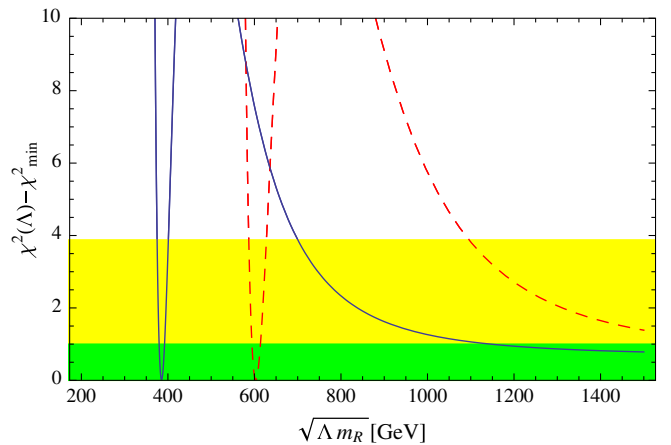

FIG. 9 (color online). The limit on the mass scale $\sqrt{\Lambda m_R}$ for the bulk RS with $L = 30$ (blue-solid line) and LRS ($L = 5$) (red-dashed line).
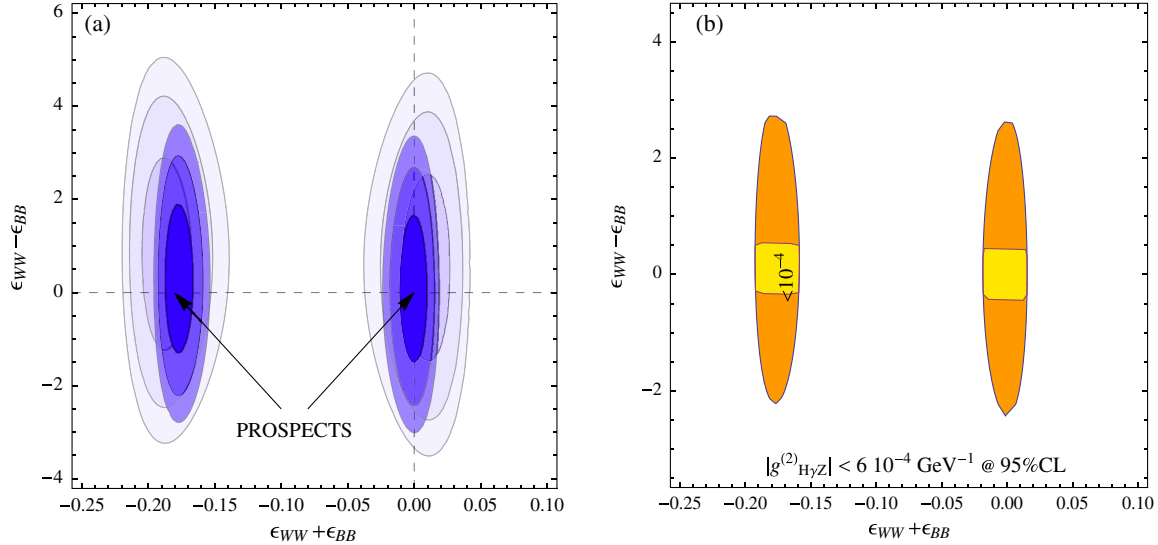
FIG. 10 (color online). (Left) Prospects on constraints from electroweak precision data and LHC data on the coefficients $\epsilon_{WW,BB}$. (Right) Prospects on the limits on the coupling of the Higgs to $Z\gamma$ in the $\epsilon_{WW,BB}$ parameter space.

$\sqrt{\Lambda m_R}$ for the RS (LRS) model. The current limit on $\sqrt{\Lambda m_R}$ is about 700 (1100) GeV, barring possible tuning into the tiny region at low mass.

Note that the radion could also couple to the gluon, and modify the Higgs production mechanism. However, for $SU(3)$, the trace anomaly becomes an important contribution, and the coupling is modified by $\propto (1 - \alpha_s bL/(2\pi))$. Here b is the total beta function of order O(1–10), depending on the localization of colored fields in the extra dimension. In this case, a partial cancellation in the radion coupling to gluons is conceivable, and could reduce its effect on the gluon fusion process.

VIII. PROSPECTS FOR THE 2012 RUN

In this section we look ahead to the end of the year's run, and how the full data set would affect the results presented in this paper. Lacking a crystal ball, we must introduce some theoretical bias. Our choice is to assume that the central values on the signal strengths $\hat{\mu}$ will move towards the SM expected values, i.e., we shall set $\hat{\mu} = 1$. Moreover, we will estimate that the error bars would go down by a factor of 2, assuming a total of 30^{-1} fb of data. This is most probably a very optimistic estimate, as some of the signal strengths are not lying around the SM value, and in migrating towards it, the errors are not expected to scale so quickly. Nevertheless, this exercise allows us to illustrate the impact of more precise data in the current analysis.

The effect on the (ϵ_W, ϵ_B) is minimal, as we display in Fig. 6(a). As the central values on WW^* and ZZ^* channels move towards the SM, the reduction of the error bars is barely affecting the global fit.

The situation for the $(\epsilon_{WW}, \epsilon_{BB})$ is more encouraging. In Fig. 10(a) we show the improvement in the fit, and in

Fig. 10(b), the improvement on the limits on g_{HAZ}, both a factor $\mathcal{O}(1.5\text{–}2)$.

IX. CONCLUSIONS

In this paper we have taken the approach that the Higgs candidate is an elementary scalar and that the leading effects of new physics appear at the level of dimension-six effective operators. We focused on four operators which affect the couplings to electroweak gauge bosons, W, Z, and γ, to constrain deviations from the SM behavior, which we named ϵ_W, ϵ_B, ϵ_{WW}, and ϵ_{BB}.

We have constrained those parameters one by one, and also by pairs ($\epsilon_{W,B}$ and $\epsilon_{WW,BB}$), as in standard scenarios of UV completions those tend to come together.

We started by looking at constraints from LEP1 (and low energy electroweak data) and LEP2, which are especially restrictive for the $\epsilon_{W,B}$ operators. After LHC data is taken into account, limits on $\epsilon_{W,B}$ do not improve significantly, and we expect no sizable improvement with the full 2012 data set.

On the other hand, the operators $\epsilon_{WW,BB}$, poorly constrained by LEP data, contribute to the Higgs to two photon coupling. The sensitivity with the current LHC data is better than LEP by a factor $\mathcal{O}(10)$. With more LHC data coming, we estimate those limits will improve by a factor of around 2.

We studied the impact of nonstandard Lorentz structures in the coupling of the Higgs to WW. As the WW^* experimental analysis makes use of angular correlations between the two leptons in the W decays, one could expect a modification of the efficiency to the cut on dilepton azimuthal angle. We found the effect is negligible, something one can qualitatively understand by realizing that the Higgs would predominantly produce parallel leptons.

We then performed a combined fit to LEP and LHC data, with no significant changes with respect to what we have already obtained using the individual channels. Namely,

limits on $\epsilon_{W,B}$ driven by LEP, whereas $\epsilon_{WW,BB}$ is mostly determined by the LHC gamma-gamma signal.

One particularly interesting anomalous coupling is the rare decay $H \rightarrow Z\gamma$. Both sets of operators can induce this coupling. We show that the limits on the decay width are at least an order of magnitude larger than the SM prediction. We then interpreted the limits in supersymmetry with light electroweak states, charged Higgses, charginos, and staus, to find that this data set is only sensitive to staus, possibly with large mixing.

Besides supersymmetry, extra-dimensional scenarios are a possible source of these operators. We have discussed the effect of the exchange of a massive radion, and set limits in terms of its mass and scale of interaction of the order of the TeV.

ACKNOWLEDGMENTS

[1] G. Aad *et al.* (ATLAS Collaboration), Phys. Lett. B **716,** 1 (2012); S. Chatrchyan *et al.* (CMS Collaboration), Phys. Lett. B **716,** 30 (2012).

[2] J. R. Espinosa, C. Grojean, M. Muhlleitner, and M. Trott, J. High Energy Phys. 05 (2012) 097; J. Ellis and T. You, J. High Energy Phys. 06 (2012) 140; 09 (2012) 123; T. Corbett, O. J. P. Eboli, J. Gonzalez-Fraile, and M. C. Gonzalez-Garcia, Phys. Rev. D **86,** 075013 (2012); J. R. Espinosa, C. Grojean, M. Muhlleitner, and M. Trott, arXiv:1205.6790; arXiv:1207.1717; A. Azatov, R. Contino, and J. Galloway, J. High Energy Phys. 04 (2012) 127; M. Montull and F. Riva, arXiv:1207.1716; M. Klute *et al.*, arXiv:1205.2699; A. Azatov, R. Contino, and J. Galloway, arXiv:1206.3171.

[3] Y. Gao, A. V. Gritsan, Z. Guo, K. Melnikov, M. Schulze, and N. V. Tran, Phys. Rev. D **81,** 075022 (2010); S. Y. Choi, D. J. Miller, M. M. Muhlleitner, and P. M. Zerwas, Phys. Lett. B **553,** 61 (2003); J. Ellis and D. S. Hwang, arXiv:1202.6660; A. De Rujula, J. Lykken, M. Pierini, C. Rogan, and M. Spiropulu, Phys. Rev. D **82,** 013003 (2010); K. Odagiri, J. High Energy Phys. 03 (2003) 009; C. P. Buszello, I. Fleck, P. Marquard, and J. J. van der Bij, Eur. Phys. J. C **32,** 209 (2004); A. Bredenstein, A. Denner, S. Dittmaier, and M. M. Weber, Phys. Rev. D **74,** 013004 (2006); P. S. B. Dev, A. Djouadi, R. M. Godbole, M. M. Muhlleitner, and S. D. Rindani, Phys. Rev. Lett. **100,** 051801 (2008); U. De Sanctis, M. Fabbrichesi, and A. Tonero, Phys. Rev. D **84,** 015013 (2011); R. Boughezal, T. J. LeCompte, and F. Petriello, arXiv:1208.4311; D. Stolarski and R. Vega-Morales, arXiv:1208.4840; J. Ellis, D. S. Hwang, V. Sanz, and T. You, arXiv:1208.6002.

[4] J. R. Espinosa, C. Grojean, V. Sanz, and M. Trott, J. High Energy Phys. 12 (2012) 077.

[5] A. Djouadi, Phys. Rep. **457,** 1 (2008).

[6] F. del Aguila, M. Perez-Victoria, and J. Santiago, Phys. Lett. B **492,** 98 (2000); J. High Energy Phys. 09 (2000) 011; F. del Aguila, J. de Blas, and M. Perez-Victoria, Phys. Rev. D **78,** 013010 (2008); J. High Energy Phys. 09 (2010) 033.

[7] K. Hagiwara, S. Ishihara, R. Szalapski, and D. Zeppenfeld, Phys. Rev. D **48,** 2182 (1993).

[8] A. De Rujula, M. B. Gavela, P. Hernandez, and E. Masso, Nucl. Phys. **B384,** 3 (1992).

[9] K. Hagiwara, S. Ishihara, R. Szalapski, and D. Zeppenfeld, Phys. Lett. B **283,** 353 (1992); O. J. P. Eboli, M. C. Gonzalez-Garcia, S. M. Lietti, and S. F. Novaes, Phys. Lett. B **478,** 199 (2000); M. C. Gonzalez-Garcia, Int. J. Mod. Phys. A **14,** 3121 (1999); F. Bonnet, M. B. Gavela, T. Ota, and W. Winter, Phys. Rev. D **85,** 035016 (2012).

[10] G. F. Giudice, C. Grojean, A. Pomarol, and R. Rattazzi, J. High Energy Phys. 06 (2007) 045.

[11] F. Bonnet, T. Ota, M. Rauch, and W. Winter, Phys. Rev. D **86,** 093014 (2012); F. Bonnet, M. B. Gavela, T. Ota, and W. Winter, Phys. Rev. D **85,** 035016 (2012).

[12] J. Beringer *et al.* (Particle Data Group), Phys. Rev. D **86,** 010001 (2012).

[13] S. Alam, S. Dawson, and R. Szalapski, Phys. Rev. D **57,** 1577 (1998).

[14] J. Erler, arXiv:1209.3324.

[15] M. E. Peskin and T. Takeuchi, Phys. Rev. D **46,** 381 (1992).

[16] G. Aad *et al.* (ATLAS Collaboration), arXiv:1210.2979.

[17] J. Erler (private communication).

[18] P. Achard *et al.* (L3 Collaboration), Phys. Lett. B **589,** 89 (2004).

[19] G. Aad *et al.* (ATLAS Collaboration), Phys. Rev. Lett. **108,** 111803 (2012).

[20] S. Chatrchyan *et al.* (CMS Collaboration), Phys. Lett. B **710,** 403 (2012).

[21] N. D. Christensen and C. Duhr, Comput. Phys. Commun. **180,** 1614 (2009).

[22] J. Alwall, M. Herquet, F. Maltoni, O. Mattelaer, and T. Stelzer, J. High Energy Phys. 06 (2011) 128.

[23] C. Degrande, C. Duhr, B. Fuks, D. Grellscheid, O. Mattelaer, and T. Reiter, Comput. Phys. Commun. **183,** 1201 (2012).

[24] T. Sjostrand, S. Mrenna, and P. Z. Skands, J. High Energy Phys. 05 (2006) 026.

[25] S. Ovyn, X. Rouby, and V. Lemaitre, arXiv:0903.2225.

[26] J. Ellis and D. S. Hwang, J. High Energy Phys. 09 (2012) 071.

[27] T. Han, Y.-P. Kuang, and B. Zhang, Phys. Rev. D **73,** 055010 (2006).

[28] Y. Takubo, R. N. Hodgkinson, K. Ikematsu, K. Fujii, N. Okada, and H. Yamamoto, arXiv:1011.5805.

[29] V. Hankele, G. Klamke, D. Zeppenfeld, and T. Figy, Phys. Rev. D **74,** 095001 (2006).

[30] T. Plehn, D. L. Rainwater, and D. Zeppenfeld, Phys. Rev. Lett. **88,** 051801 (2002).

[31] D. Stolarski and R. Vega-Morales, Phys. Rev. D **86,** 117504 (2012).

[32] G. Aad *et al.* (ATLAS Collaboration), Phys. Lett. B **716,** 62 (2012).

[33] S. Chatrchyan *et al.* (CMS Collaboration), Phys. Lett. B **710,** 91 (2012).

[34] G. Aad *et al.* (ATLAS Collaboration), Phys. Lett. B **710,** 383 (2012).

[35] S. Chatrchyan *et al.* (CMS Collaboration), Phys. Rev. Lett. **108,** 111804 (2012).

[36] J. S. Gainer, W.-Y. Keung, I. Low, and P. Schwaller, Phys. Rev. D **86,** 033010 (2012).

[37] A. Djouadi, V. Driesen, W. Hollik, and A. Kraft, Eur. Phys. J. C **1,** 163 (1998).

[38] A. Djouadi, V. Driesen, W. Hollik, and J. I. Illana, Eur. Phys. J. C **1,** 149 (1998).

[39] C. Csaki, J. Hubisz, and S. J. Lee, Phys. Rev. D **76,** 125015 (2007).

[40] H. Davoudiasl, G. Perez, and A. Soni, Phys. Lett. B **665,** 67 (2008).